iScience

CellPress
OPEN ACCESS

Article

# High-entropy $R_2O_3$-$Y_2O_3$-$TiO_2$-$ZrO_2$-$Al_2O_3$ glasses with ultrahigh hardness, Young's modulus, and indentation fracture toughness

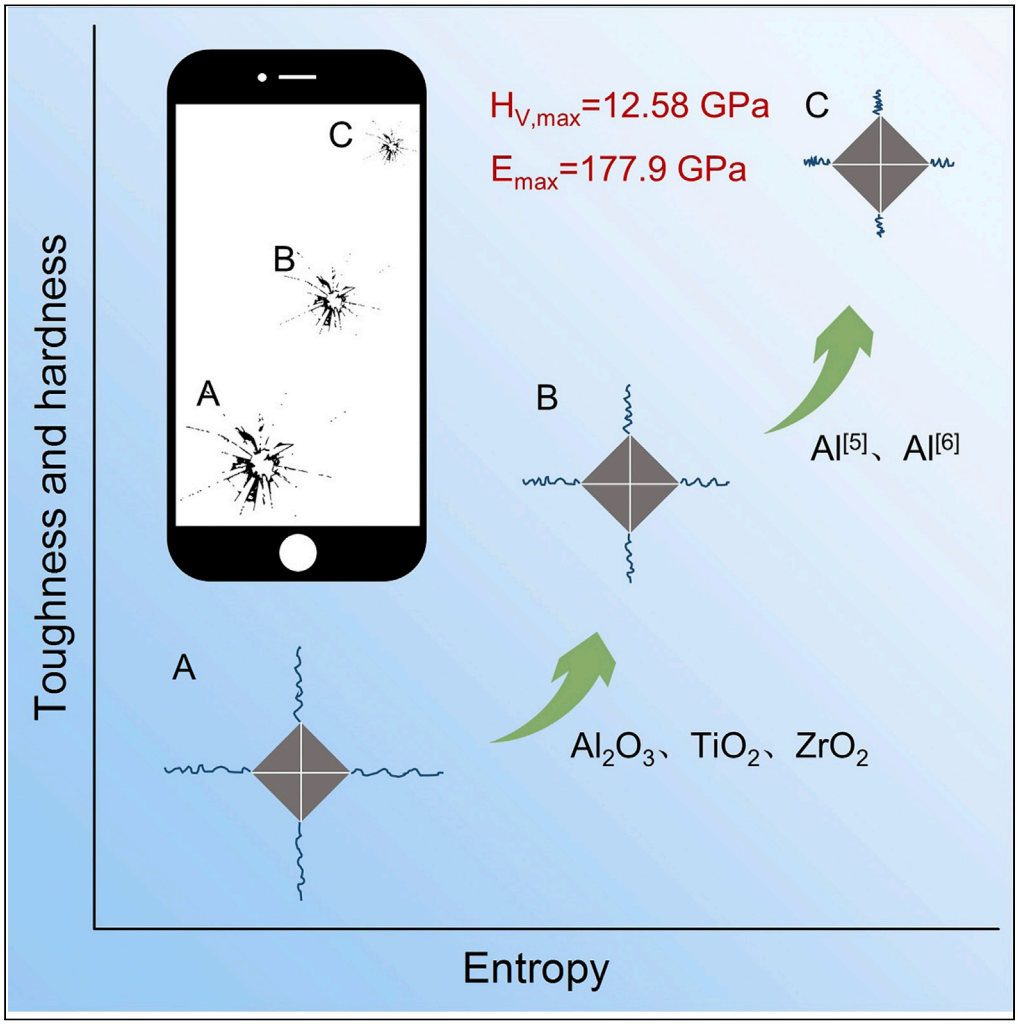


Yongchang Guo, Jianqiang Li, Ying Zhang, Shaowei Feng, Hong Sun

jqli@ipe.ac.cn

## Highlights

The conceptual design of high-entropy materials is firstly extended to oxide glass

The as-prepared oxide glass possesses the record hardness and Young's modulus

The as-prepared oxide glass exhibits excellent indentation fracture toughness

The distinct mechanical properties relate to componential multiplicity of the glass

Guo et al., iScience *24*, 102735
July 23, 2021 
https://doi.org/10.1016/j.isci.2021.102735

iScience

CellPress
OPEN ACCESS

Article

# High-entropy $R_2O_3$-$Y_2O_3$-$TiO_2$-$ZrO_2$-$Al_2O_3$ glasses with ultrahigh hardness, Young's modulus, and indentation fracture toughness

Yongchang Guo,[1,3] Jianqiang Li,[1,2,3,4,5,*] Ying Zhang,[1,3] Shaowei Feng,[1,3] and Hong Sun[1,3]

## SUMMARY

**Glasses with high hardness, high Young's modulus, and high fracture toughness become crucial materials which are urgently needed in the protective covers for various electronic displays. Here, a paradigm is presented that the conceptual design of high-entropy materials is adaptable to high performance oxide glasses. We designed the multi-component glass compositions of $18.77R_2O_3$-$4.83Y_2O_3$-$28.22TiO_2$-$8.75ZrO_2$-$39.43Al_2O_3$ (R = La, Sm, Gd) and elaborated successfully the glassy samples through a containerless solidification process. The as-prepared samples demonstrated the outstanding mechanical and optical properties. The measured hardness, Young's modulus, and indentation fracture toughness of the high-entropy (R = Gd) glass are 12.58 GPa, 177.9 GPa, and 1.52 MPa·$m^{0.5}$, respectively, in which the hardness and Young's modulus exhibit the highest value among the reported oxide glasses. Structural analysis revealed that the excellent mechanical properties are attributed to the large dissociation energies and the high field strength of $Al_2O_3$, $TiO_2$, and $ZrO_2$ and the complex interaction between atoms caused by high entropy.**

## INTRODUCTION

Glasses with high hardness, high Young's modulus, and high fracture toughness have a wide range of applications in the protective covers for electronic displays on smartphones, laptops, tablets, and wearable devices owing to their high resistance to scratching and sharp contact damage. Cover glasses are the outermost layer of electronic displays and the most vulnerable part of wearable devices under external force. Higher hardness, Young's modulus, and fracture toughness are able to reduce the glass thickness while retaining sufficient durability. In order to enhance the conventional cover glasses, such as soda lime silicate ($Na_2O$-CaO-$SiO_2$) glass and alkali alumina-silicate ($R_2O$-$Al_2O_3$-$SiO_2$) glass, chemical strengthening is widely used and the mechanical properties are improved by an ion exchange process (Nordberg et al., 1964; Morozumi et al., 2015). However, the shape design is limited, and it is difficult to reprocess once the glass is chemically strengthened; most importantly, the chemical strengthening is not the internal mechanical strengthening. Transparent ceramics and glass-ceramics have been developed in the latest decade and recognized as competing materials with cover glass. They demonstrate the natural higher hardness, Young's modulus, and fracture toughness compared to glasses; however, the extremely high cost and complex process of ceramics and glass-ceramics still restrain the cost-efficient application of these crystalline products. Accordingly, synthesizing glasses with intrinsically high hardness, high Young's modulus, and high fracture toughness is of great significance.

The Young's modulus $E$ of glass can be estimated by the Makishima and Mackenzie equation (Makishima, 1973), in which $E$ is in proportion to the atomic packing density and the sum of the dissociation energy of each component. The Vickers hardness $H_V$ of glass was in association with Young's modulus by Yamane and Mackenzie equation (Yamane and Mackenzie, 1974) in which $H_V$ is in proportion to $E$. For the fracture toughness of glass, the bond energies of oxides are the most important factors, which can be expressed in terms of the dissociation energy. Therefore, in order to obtain glass with high hardness, high Young's modulus, and high fracture toughness, the atomic packing density and the dissociation energy of components are primary factors for glass composition design. Among metallic oxides, alumina ($Al_2O_3$) possesses the highest dissociation energy ($G_{Al2O3}$ = 133.8 kJ/$cm^3$) (Makishima, 1973). Hence, it is reasonable that the glasses with high hardness, high Young's modulus, and high fracture toughness contain a great quantity of $Al_2O_3$,

[1]CAS Key Laboratory of Green Process and Engineering, National Engineering Laboratory for Hydrometallurgical Cleaner Production Technology, Institute of Process Engineering, Chinese Academy of Sciences, Beijing 100190, P. R. China

[2]School of Materials Science and Engineering, University of Science and Technology Beijing, Beijing 100083, P. R. China

[3]University of Chinese Academy of Sciences, Beijing 100049, P. R. China

[4]Innovation Academy for Green Manufacture, Chinese Academy of Sciences, Beijing 100190, P. R. China

[5]Lead contact

*Correspondence: jqli@ipe.ac.cn

https://doi.org/10.1016/j.isci.2021.102735

as reported in $R_2O_3$-$Al_2O_3$-$SiO_2$ glasses (R = rare earth ion, Y, or Sc) and 25Li2O-20Al2O3-55B2$O_3$ glass (Stevensson and Edén, 2013; Johnson et al., 2005; Du, 2009; Inaba et al., 2000; To et al., 2021). The atomic packing density of glass increases with the coordination number of Al and decreases with the ionic volume of oxide components. The coordination number of Al in glasses could be improved by introducing the high field strength cations into the network. For example, Mattias and Masuno et al. found that rare earth ions/$Y^{3+}$/$Sc^{3+}$ (Yamane and Mackenzie, 1974; Stevensson and Edén, 2013; Johnson et al., 2005; Du, 2009; Inaba et al., 2000) or $Ta^{5+}$ (Rosales-Sosa et al., 2015) in the aluminate glasses can significantly increase the fraction of high-coordinated Al. Therefore, selecting components with high field strength, coupled with a higher $Al_2O_3$ content, is expectable to get larger Al coordination and enhance the mechanical properties of oxide glasses. Masuno et al. prepared the 32$R_2O_3$-68$Al_2O_3$ glasses (R = La, Sm, Gd, Er, Tm, Y), which possess the maximum hardness at the time among oxide glasses (between 8.4 GPa and 11.1 GPa) (Rosales-Sosa et al., 2018). However, as an intermediate oxide, the existence of a large amount of $Al_2O_3$ would result in the decrease of the glass-forming ability and, more severely, the failure of vitrification of high alumina-contained glasses (Sun, 1947). Adding a certain amount of $SiO_2$ enables to improve the glass-forming ability (Han et al., 2019); however, the glasses would be impaired by the decreased mechanical properties and relatively low dopant concentrations (Johnson et al., 2005; Hehlen et al., 1997). Currently, with the rapid development of electronic equipment, seeking an alternative way to obtain the high hardness, high modulus, and high fracture toughness glasses becomes more urgent.

Recently, the concept of high entropy is widely concerned and studied in alloys and ceramics. Usually, the high-entropy materials are considered to be composed of five or more components, and the mole fraction of each component is between 5% and 35% (Yeh et al., 2004). It exhibits extraordinary properties compared to the traditional materials due to the existence of the four effects which included high-entropy effect (Tong et al., 2005; Li and Zhang, 2009; Senkov et al., 2010; Del Grosso et al., 2012; Ng et al., 2012; Lucas et al., 2012), sluggish diffusion effect (Cheng et al., 2006; Tsai et al., 2013), lattice distortion effect, and cocktail effect (Ranganathan, 2003; Yeh, 2006; Zhao et al., 2020). Among that, lattice distortion effect is unique to crystals and cocktail effect is the total change in performance, which has no remarkable influence on glasses because of the random amorphous distribution atoms. The reported work on high-entropy metallic glasses demonstrates that the complex interaction between atoms due to the diversity of components can improve the hardness and compressive strength of glasses (Kim et al., 2020). Additionally, the increase of entropy can improve the stability of amorphous in thermodynamics and therefore improve the glass-forming ability (Li and Zhang, 2017). Meanwhile, the effect of sluggish diffusion caused by the complex interaction between atoms can also promote the formation of amorphous by increasing the viscosity of the glass melts.

Herein, based on the multicomponent compositional design, we elaborated successfully the high-entropy 18.77$R_2O_3$-4.83$Y_2O_3$-28.22$TiO_2$-8.75$ZrO_2$-39.43$Al_2O_3$ (R = La, Sm, Gd) glasses which are containerlessly molten and solidified by using an aerodynamic levitation process. The optical, thermal, and physical properties of glasses are investigated. Results demonstrate that the prepared high-entropy glass possesses ultrahigh hardness, Young's modulus, and fracture toughness, coupled with good thermal stability and excellent transmittance performance. The conceptual design of high-entropy glasses can be extended to the system of high hardness, high Young's modulus, and high fracture toughness glasses, targeting wide applications in the protective covers for electronic displays on smartphones, laptops, tablets, and wearable devices.

## RESULTS AND DISCUSSION

### Vitrification of high-entropy aluminates

The cooling curves of the levitated melts with high-entropy 18.77$R_2O_3$-4.83$Y_2O_3$-28.22$TiO_2$-8.75$ZrO_2$-39.43$Al_2O_3$ (R = La, Sm, Gd) compositions are given in Figure 1A, in which the inset picture shows three as-prepared samples. The temperature of samples decreased at the cooling rate of approximately 175 K/s once turning off the lasers. No recalescence is observed on the cooling curves. All of the samples are transparent and colorless except for R = Sm glass with light yellow. Figure 1B presents the X-ray diffraction patters of the samples, and only a unique amorphous peak is found. Therefore, it is reasonable to deduce that the as-prepared samples are in glassy state.

To verify the morphology of the elemental distribution of the high-entropy glasses, scanning electron microscope (SEM) observation and corresponding energy dispersive spectroscopy (EDS) mapping of samples are performed in R = La glass. Energy spectrum analysis (Figure 1C) shows that the glass samples consist of six elements including La, Ti, Zr, Y, Al, and O, which is consistent with the nominal composition and no other

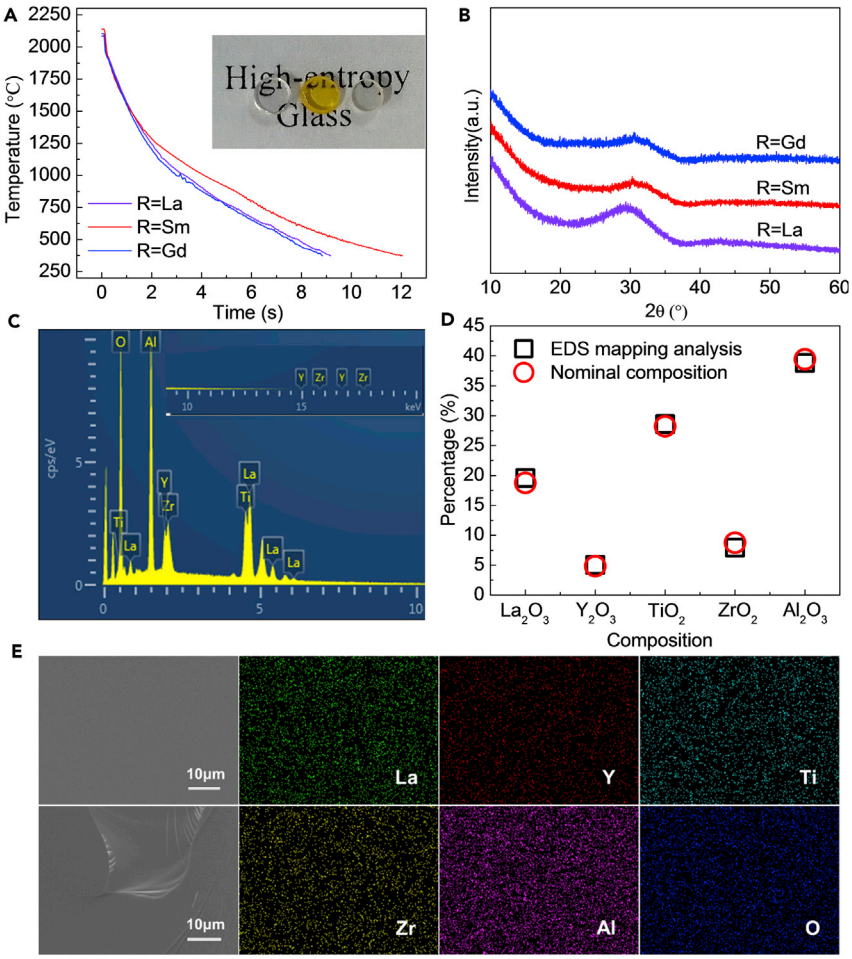


**Figure 1. Amorphous characterization of the high-entropy $18.77R_2O_3$-$4.83Y_2O_3$-$28.22TiO_2$-$8.75ZrO_2$-$39.43Al_2O_3$ (R = La, Sm, Gd) glasses**

(A) Solidification cooling curves of the as-synthesized glass samples, and the inset picture shows the prepared glass beads, which are transparent and colorless except for R = Sm glass which is light yellow.

(B) X-ray diffraction patters of the glass samples. Results demonstrate that the as-synthesized high-entropy glasses are all completely amorphous.

(C) Energy spectrum diagram of R = La glass sample.

(D) Comparison of measured and nominal composition of each component in R = La glass sample.

(E) SEM image and corresponding EDS mapping of the high-entropy glasses (R = La). The elements are homogenously distributed.

impurity ions are observed. Figure 1D shows a comparison of measured and nominal composition of each component, and it is clear that all of the measured composition is highly consistent with the ingredients. Figure 1E shows the SEM image and corresponding EDS mappings of the high-entropy glass (R = La). The surface and fracture of samples are smooth, homogeneous, crack free, and dense. EDS mappings on the polished surface indicate that all of the elements are homogenously distributed at the microscale and no phase separation is observed.

## Thermal analysis

The complexity of preparing glasses in bulk depends on the thermal stability and glass-forming ability of amorphous. Figure 2A shows the differential thermal analysis (DTA) curves of the high-entropy $18.77R_2O_3$-$4.83Y_2O_3$-$28.22TiO_2$-$8.75ZrO_2$-$39.43Al_2O_3$ (R = La, Sm, Gd) glasses. The glass transition temperature $T_g$, crystallization temperature $T_P$, and kinetic window $\Delta T$ ($\Delta T = T_P$-$T_g$) are obtained from DTA curves, which are illustrated in Figure 2B. The glass transition temperature $T_g$ and the crystallization temperature $T_p$ for R = La, Sm, and Gd glass are 832°C, 849°C, and 862°C and 918°C, 919°C, and 925°C, respectively. The

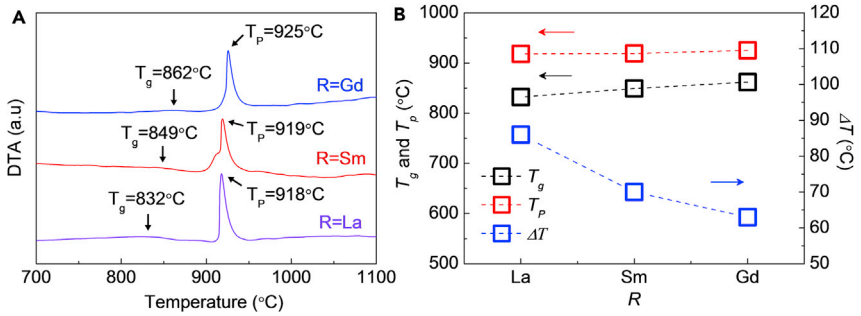


**Figure 2. Thermal stability and glass forming ability of the high-entropy $18.77R_2O_3$-$4.83Y_2O_3$-$28.22TiO_2$-$8.75ZrO_2$-$39.43Al_2O_3$ (R = La, Sm, Gd) glasses**

(A) Differential thermal analysis (DTA) curves of the glass samples.

(B) The glass transition temperature $T_g$, crystallization temperature $T_P$, and kinetic window $\Delta T$ ($\Delta T = T_P$-$T_g$) of R = La, Sm, and Gd glass samples.

Results demonstrate that the as-synthesized glasses have a good thermal stability and strong glass-forming ability.

temperature difference between $T_g$ and $T_P$ ($\Delta T = T_P - T_g$) for R = La, Sm, and Gd glass is 86°C, 70°C, and 63°C, respectively. The temperature difference $\Delta T$ is a measurement of the thermal stability of glass, which is also closely related to the glass-forming ability and determines the possibility of bulk glass preparation.

In this work, the $\Delta T$ of the obtained glass samples is all larger than 60°C and reached the maximum 86°C when R = La, which is much higher than that of previous work on $54Al_2O_3$-$46Ta_2O_5$ glasses ($\Delta T$ = 54°C) (Rosales-Sosa et al., 2015). The higher $\Delta T$ indicates that the as-synthesized glasses possess a better thermal stability and stronger glass-forming ability, these make it possible that prepare bulk glasses without network former. Compared with the $54Al_2O_3$-$46Ta_2O_5$ glass, the higher $\Delta T$ can be partially contributed to the lower $Al_2O_3$ content. As an intermediate oxide, less $Al_2O_3$ amount in our high-entropy glasses will lead to low coordinated Al and thus higher bond strength, according to Sun's glass formation criteria (Sun, 1947), which is beneficial to increase the glass stability. Additionally, the complex interaction between atoms caused by high entropy may also play a role in the promotion of $\Delta T$. The entropy of the prepared high-entropy glasses is calculated as 10.95 $J \cdot mol^{-1} \cdot K^{-1}$ and is much higher than that of the $54Al_2O_3$-$46Ta_2O_5$ glass (5.74 $J \cdot mol^{-1} \cdot K^{-1}$); higher entropy indicates that atomic interactions in glass systems are more complex. In the melting state, the sluggish diffusion of atoms can lead to an increase in the viscosity of the glass melt, making it easier to form glass during solidification.

## Optical properties

Optical transmittance is one of the most important parameters for cover glasses used for electronic displays; therefore, transparent and colorless cover glasses are both indispensable. R = Sm glass is transparent but with a light yellow color; hence, the optical transmittance of glass in 190–2500 nm and 2500–7000 nm wavelength range is only performed in R = La and Gd glass. Figure 3 shows the transmittance spectrum of the high-entropy $18.77R_2O_3$-$4.83Y_2O_3$-$28.22TiO_2$-$8.75ZrO_2$-$39.43Al_2O_3$ (R = La, Gd) glasses in the UV-visible (Figure 3A) and NIR region (Figure 3B). From the figure, it can be observed that both R = La and Gd glass had a good transmittance in the UV-visible and NIR region. The transmittance at 390 nm–780 nm is higher than 80% for R = La glass, and it has a maximum transmission of 86.8% in the visible region. For R = Gd glass, the transmittance at 390 nm–780 nm and the largest transmission in the visible region are 76.9% and 84.0%, respectively. The transmittance of the obtained glass samples is much higher than that of the previous high hardness and high Young's modulus glass on $54Al_2O_3$-$46Ta_2O_5$ (81%) (Rosales-Sosa et al., 2015), although the latter is half as thick as the former. By comparison, the as-synthesized glasses have a wide range of transmission windows in visible and near infrared regions except R = Sm glass, and the cutoff wavelengths of UV and infrared for both glasses are about 325 nm and 6813 nm, respectively. The absorption band at approximately 4250 nm for R = La and Gd belongs to the vibration of ambient $CO_2$ (Ma et al., 2015).

## Mechanical properties

### *Hardness and Young's modulus*

The hardness and Young's modulus of the as-synthesized high-entropy $18.77R_2O_3$-$4.83Y_2O_3$-$28.22TiO_2$-$8.75ZrO_2$-$39.43Al_2O_3$ (R = La, Sm, Gd) glasses are measured, and the results are illustrated in Figure 4.

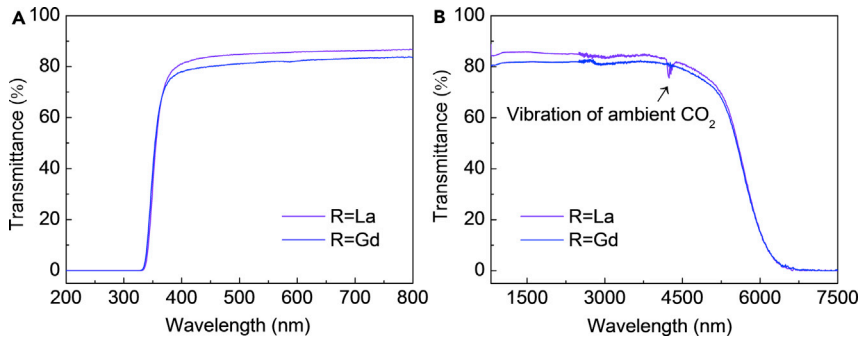


**Figure 3. Optical properties of the high-entropy $18.77R_2O_3$-$4.83Y_2O_3$-$28.22TiO_2$-$8.75ZrO_2$-$39.43Al_2O_3$ (R = La, Gd) glasses**

(A) Transmittance spectrum of the glasses in the UV-visible region.

(B) Transmittance spectrum of the glasses in the NIR region.

Results demonstrate that the as-synthesized high-entropy glasses possess a higher transmittance in the UV-visible region than the previous high hardness and high Young's modulus glass on $54Al_2O_3$-$46Ta_2O_5$ (81%) (Rosales-Sosa et al., 2015).

The hardness and Young's modulus fluctuate greatly when the displacement of the surface is smaller than 500 nm and then became stabilized while the pressure depth is increased to 900 nm (Figures 4A and 4B). This can be due to the presence of surface stress when the pressure depth is relatively shallow, and the intrinsic hardness of glass is obtained while the pressing depth is larger than 900 nm. The hardness and Young's modulus increase while the R in the glasses changes from La to Gd. Figure 4C shows the load displacement into the surface curve of glass samples, and it also revealed that the hardness increases with the R = La to Gd as the load increases continuously at the same pressure depth. The measured hardness and Young's modulus of glasses are summarized in Table 1.

Vickers hardness ($H_V$) versus Young's modulus ($E$) for high-entropy $18.77R_2O_3$-$4.83Y_2O_3$-$28.22TiO_2$-$8.75ZrO_2$-$39.43Al_2O_3$ (R = La, Sm, Gd) glasses in comparison with those of other high performance oxide glasses are presented in Figure 4D (Rosales-Sosa et al., 2015, 2016, 2018; Segawa et al., 2010). For the most oxide glasses, their hardness and Young's modulus are lower than 10 GPa and 140 GPa. The hardness of the prepared high-entropy glass is in the range of 11.65 GPa–12.58 GPa, and the Young's modulus of the prepared high-entropy glass is between 162.0 GPa and 177.9 GPa, which are considerably larger than the values of conventional oxide glass. To our knowledge, the reported maximum values of hardness and Young's modulus are obtained on $32R_2O_3$-$68Al_2O_3$ glasses, whose hardness is between 8.4 GPa and 11.1 GPa, with the Young's modulus of 122.3 GPa–162.9 GPa (Rosales-Sosa et al., 2018). Specifically, the obtained glass samples in this work exhibit much higher values than the $32R_2O_3$-$68Al_2O_3$ glasses except the Young's modulus of R = La glass (162.0 GPa). The comparison shows that the high-entropy $18.77R_2O_3$-$4.83Y_2O_3$-$28.22TiO_2$-$8.75ZrO_2$-$39.43Al_2O_3$ (R = La, Sm, Gd) glasses exhibit the superior hardness and Young's modulus among the oxide glasses.

### *Indentation fracture toughness*

Glasses with high hardness and Young's modulus can effectively improve the crack initiation resistance and reduce the probabilities of sharp contact damage of cover glass. However, once the collapsing force is high enough and results in the crack nucleation or the flaws and cracks are pre-existing on the surface, the fracture toughness of glass is of great important in resisting the growth of flaws and cracks. Here, Vickers indentation is used to identify the fracture toughness of the as-synthesized high-entropy $18.77R_2O_3$-$4.83Y_2O_3$-$28.22TiO_2$-$8.75ZrO_2$-$39.43Al_2O_3$ (R = La, Sm, Gd) glasses, and the results are shown in Figure 5. Figure 5A shows the diagrammatic sketch of the measurement on the crack length, and the inset pictures show the scanning electron micrographs of indentations performed in R = La, Sm, and Gd glass. The indentation is square like, and the cracks are extended at the end of four corners; there are no ring-type cracks observed on the surface, which indicated that the selected load is appropriate and the effect of densification flow on testing during the indentation process is reduced in visibility.

The measured fracture toughness ($K_{IC}$) and average crack length ($c$-$a$) of glass samples are shown in Figure 5B. The fracture toughness of the high-entropy glasses increase with R changing from La to Gd; conversely, the

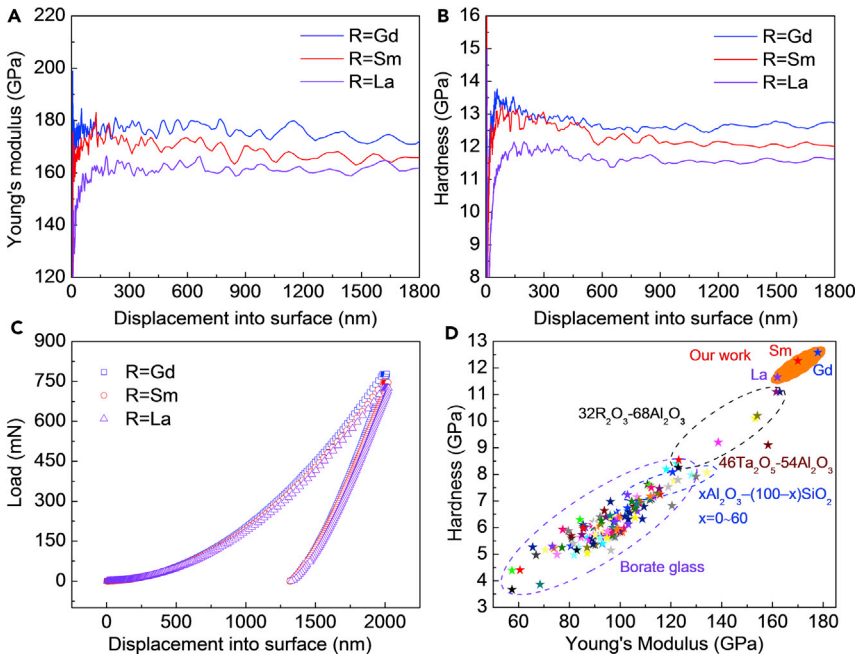


**Figure 4. Hardness and Young's modulus of the high-entropy $18.77R_2O_3$-$4.83Y_2O_3$-$28.22TiO_2$-$8.75ZrO_2$-$39.43Al_2O_3$ (R = La, Sm, Gd) glasses**

(A) The measured Young's modulus displacement into surface curve of the glass samples.

(B) The measured Vickers hardness displacement into surface curve of the glass samples.

(C) The obtained load displacement into surface curve of the glass samples.

(D) Vickers hardness ($H_V$) versus Young's modulus ($E$) for as-synthesized high-entropy glasses together with some high hardness and high Young's modulus glasses.

Results demonstrate that the as-synthesized high-entropy glass possesses the highest hardness and Young's modulus among oxides glass.

crack length decreases as R goes from La to Gd. Under the same load, glasses with higher fracture toughness can exhibit stronger resistance to crack growth, and this results in the decrease of crack length. Notably, the fracture toughness of R = La, Sm, and Gd glass is 1.21 MPa·$m^{0.5}$, 1.39 MPa·$m^{0.5}$, and 1.52 MPa·$m^{0.5}$, respectively, which is much larger than the values of current commercially available oxide glasses, such as silicates, borates, borosilicate, etc., which is reported to be lower than 1 MPa·$m^{0.5}$ (Quinna and Swab, 2013; To, 2019; Østergaard et al., 2019; Rouxel and Yoshida, 2017; Yao, 2016; Scannell et al., 2017; Vullo and Davis, 2004; Wiederhorn et al., 1974; Mezeix, 2017; Kato et al., 2010; Reddy et al., 1988), as shown in Figure 5C (areas below the gray short dash line). Currently, the highest fracture toughness of oxide glasses is reported to be 1.36 MPa $m^{0.5}$ using the single-edge pre-cracked beam method (To et al., 2021). In this work, the measured fracture toughness of R = Sm and Gd glass exhibits an almost comparable value to that of maximum record. Generally, there are errors in the fracture toughness measured by indentation methods, the overestimated values for silicate-rich glasses and underestimated values for stiffer and harder glasses (Dériano et al., 2004). However, it can be considered that the prepared high-entropy glasses possess extraordinary fracture toughness owing to its silicate-free and extremely high hardness and Young's modulus of glass samples. The prepared high hardness, high Young's modulus, and high fracture toughness $18.77R_2O_3$-$4.83Y_2O_3$-$28.22TiO_2$-$8.75ZrO_2$-$39.43Al_2O_3$ (R = La, Sm, Gd) glasses, coupled with their good glass-forming ability and excellent transmission performance, indiacte a great potential application on the future's electronic devices.

## Structural analysis

### *Hardness and Young's modulus*

The atomic packing density and the dissociation energy of components are the most important two factors to synthesize the high hardness and high Young's modulus glasses. For the prepared high-entropy $18.77R_2O_3$-$4.83Y_2O_3$-$28.22TiO_2$-$8.75ZrO_2$-$39.43Al_2O_3$ (R = La, Sm, Gd) glasses, it is noted that the measured hardness (12.58 GPa) and Young's modulus (177.9 GPa) of R = Gd glass are much larger than

**Table 1. Ionic radii of *R* (R = La, Sm, Gd) cations, density ($\rho$), atomic packing density ($C_g$), Young's modulus ($E$), and Vickers hardness ($H_V$) of the high-entropy $18.77R_2O_3$-$4.83Y_2O_3$-$28.22TiO_2$-$8.75ZrO_2$-$39.43Al_2O_3$ (R = La, Sm, Gd) glasses**

| *R* | Ionic radii[a]/nm | $\rho$/(g/cm$^3$) | $C_g$ | *E*/GPa | $H_V$/GPa |
|---|---|---|---|---|---|
| La | 0.1061 | 4.565 | 0.5711 | 162.0 | 11.65 |
| Sm | 0.0964 | 4.831 | 0.5780 | 170.0 | 12.26 |
| Gd | 0.0938 | 5.011 | 0.5871 | 177.9 | 12.58 |

The radius of the oxide ion is 1.35 Å. The maximum standard deviation of the Young's modulus *E* and Vickers hardness $H_V$ was within $\pm$0.8 GPa and $\pm$0.06 GPa, respectively.
[a]Shannon ionic radii for sixfold coordination.

those of the $32R_2O_3$-$68Al_2O_3$ glass, which is reported to have the highest values among oxide glasses (when R = Er possess the highest hardness 11.1 GPa and Young's modulus 162.9 GPa) (Rosales-Sosa et al., 2018). All of the prepared high-entropy glasses have the same component except $R_2O_3$; therefore, the increased hardness and Young's modulus of glass samples from R = La to Gd can be owing to the difference in $R_2O_3$. Inaba et al. reported that different rare-earth oxides have the similar dissociation energy (60–70 kJ/cm$^3$), and the dissociation energy is not directly related to the ion radius (Inaba et al., 2000). The increased hardness and Young's modulus values of $18.77R_2O_3$-$4.83Y_2O_3$-$28.22TiO_2$-$8.75ZrO_2$-$39.43Al_2O_3$ (R = La, Sm, Gd) glasses are thus caused by the different atomic packing density. The measured density and the calculated atomic packing density $C_g$ of the glass samples are listed in Table 1; Figures 6A and 6B show their variation with the ionic radii of R (R = La, Sm, Gd) cations. From the figure, it can be observed that the density and the atomic packing density $C_g$ of glasses are increased with the decrease of the ionic radii, which indicated that selecting components with smaller ionic radii is conducive to increase the atomic packing density $C_g$. Figure 6C illustrates the effect of the atomic packing density ($C_g$) on Vickers hardness and Young's modulus of glass. It can be observed that both values are monotonically increased with the packing density $C_g$. Accordingly, the increased hardness and Young's modulus of glass samples from R = La to Gd is owing to the decreased ionic radii, which is consistent with the previous work on $32R_2O_3$-$68Al_2O_3$ glasses (R = La, Sm, Gd, Er, Tm, Y) (Rosales-Sosa et al., 2015). Compared with the previous high hardness and high Young's modulus oxide glasses, such as $Al_2O_3$-$SiO_2$-$R_2O_3$, $54Al_2O_3$-$46Ta_2O_5$, $32R_2O_3$-$68Al_2O_3$, and $Al_2O_3$–$SiO_2$ (Inaba et al., 2000; Rosales-Sosa et al., 2015, 2016, 2018), the improved hardness and Young's modulus of the as-synthesized high-entropy glasses can be partially contributed to the increased atomic packing density $C_g$. The atomic packing density $C_g$ of the obtained glass samples varies from 0.5711 to 0.5871, and while changing the cations R from La to Gd, these values were much larger than those of the conventional silicate glasses and the majority of high hardness and high Young's modulus glasses (Inaba et al., 2000; Rosales-Sosa et al., 2015, 2018). Additionally, the addition of $ZrO_2$ and $TiO_2$ can also improve the hardness and Young's modulus, whose dissociation energy is much larger than that of rare-earth oxides and silicon dioxide (Makishima, 1973; Inaba et al., 2000). Entropy may also affect the hardness and modulus of oxide glasses, although it has not been reported so far in oxide glass, and the relevant research has been confirmed in metallic glass (Argon, 1979; Chen et al., 2015; Kim et al., 2020). For low-entropy glasses, the shear deformation resistance of glass is relatively small owing to the simple atomic interaction. For high-entropy glasses, there is a complex interaction between atoms due to the diversity of components, which make atomic motion and shearing more difficult than conventional oxide glasses with simple atomic interaction during compressive deformation.

The atomic packing density $C_g$ is positively correlated with the coordination of Al. Thus, to identify the coordination information of glass samples, 27Al NMR spectroscopy is performed in R = La glass, and the results are presented in Figure 6D. Although all of the spectrums are broad owing to the amorphous nature of the glass, three distinctive peaks are observed in about 75 ppm, 45 ppm, and 10 ppm. These peaks are assigned to 4-coordinated Al ($Al^{[4]}$), 5-coordinated Al ($Al^{[5]}$), and 6-coordinated Al ($Al^{[6]}$), respectively (Schmücker et al., 1999; Neuville et al., 2006; Licheron et al., 2011). For a better study of the coordination condition of the glass, Gaussian fitting is used to quantify the fraction of Al coordination species. The thin dash in the spectrum corresponds to each of the components: blue dash ($Al^{[4]}$), green dash ($Al^{[5]}$), and black dash ($Al^{[6]}$). Based on the integration of the peak areas, the fractions of 4-coordinated Al ($Al^{[4]}$), 5-coordinated Al ($Al^{[5]}$), and 6-coordinated Al ($Al^{[6]}$) are estimated to be 55.3%, 31.0%, and 13.7%, respectively. The estimated average oxygen coordination number for Al is 4.584. High oxygen coordination number

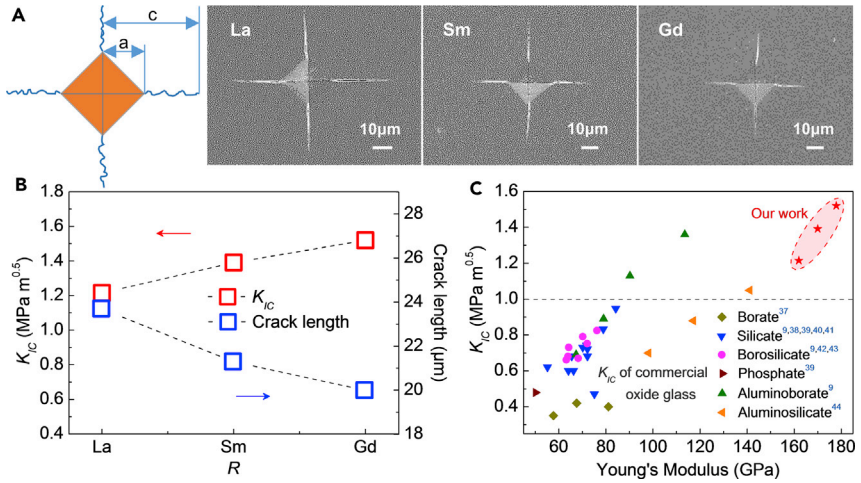


**Figure 5. Fracture toughness ($K_{IC}$) of the high-entropy 18.77$R_2O_3$-4.83$Y_2O_3$-28.22$TiO_2$-8.75$ZrO_2$-39.43$Al_2O_3$ (R = La, Sm, Gd) glasses**

(A) Diagrammatic sketch of the measurement on the crack length for fracture toughness ($K_{IC}$), and the inset pictures show the scanning electron micrographs of indentations performed on R = La, Sm, and Gd glass.

(B) The fracture toughness ($K_{IC}$) and average crack length (C-A) of R = La, Sm, and Gd glass samples.

(C) Fracture toughness ($K_{IC}$) versus Young's modulus ($E$) for as-synthesized high-entropy glasses together with some commercial oxide glasses and high fracture toughness oxide glasses.

Results demonstrate that the as-synthesized high-entropy glass possesses extraordinary fracture toughness among oxides glass.

for Al ($Al^{[5]}$, $Al^{[6]}$) can improve the atomic packing density $C_g$ of glass and thus obtain excellent mechanical properties. The fractions of 5-coordinated Al ($Al^{[5]}$) and 6-coordinated ($Al^{[6]}$) for conventional aluminates glasses generally ranged from 3 to 30% and from 1 to 2%, respectively (Pahari et al., 2012; Takahashi et al., 2015; Tangeman et al., 2004), which are considerably smaller than those of the prepared high-entropy glasses, especially for 6-coordinated ($Al^{[6]}$). It has been suggested that the amount of $Al^{[5]}$ and $Al^{[6]}$ in aluminate glasses can be improved by the cations with high field strength (Stevensson and Edén, 2013; Johnson et al., 2005; Du, 2009; Inaba et al., 2000; Rosales-Sosa et al., 2015). $Ti^{4+}$ and $Zr^{4+}$ cations possess larger field strength compared with rare-earth cations due to the higher valence and smaller ionic radii. Accordingly, the increased highly coordinated aluminum ($Al^{[5]}$ and $Al^{[6]}$) can be owing to the addition of $Ti^{4+}$ and $Zr^{4+}$ cations, which results in the larger atomic packing density $C_g$ and thus improves the hardness and Young's modulus.

### *Indentation fracture toughness*

Fracture toughness ($K_{IC}$) represents the ability of a material to prevent crack propagation, similar to hardness and Young's modulus, and it is highly related to the bond energy of component oxides and the density of obtained glass samples. As presented in Figure 5B, the fracture toughness of the high-entropy glasses increases with R changing from La to Gd. This can be partly owing to the increased glass density from R = La to Gd (Figures 6A and 6B). On the other hand, a decrease in the ionic radii of R increases the bond energy, and more energies are needed to crack extending, which result in the enhancement of fracture toughness. As presented in Figure 5C, the prepared high-entropy glasses exhibit extraordinary fracture toughness compared with the commercial oxide glasses (borates, silicates, borosilicates, etc. [To et al., 2021; Yao, 2016; Scannell et al., 2017; Vullo and Davis, 2004; Wiederhorn et al., 1974; Mezeix, 2017; Kato et al., 2010; Reddy et al., 1988]) and the current high fracture toughness oxide glasses (To et al., 2021; Dériano et al., 2004). The dissociation energy of the widely used oxides on conventional glasses, such as $B_2O_3$, $SiO_2$, $P_2O_5$, and alkali metal oxides, is 77.8 kJ/cm$^3$, 64.4 kJ/cm$^3$, 62.7 kJ/cm$^3$, and 23.4–83.6 kJ/cm$^3$, (23.4 kJ/cm$^3$ for $K_2O$, 37.2 kJ/cm$^3$ for $Na_2O$, 40.5 kJ/cm$^3$ for BaO, 48.5 kJ/cm$^3$ for SrO, 64.8 kJ/cm$^3$ for CaO, and 83.6 kJ/cm$^3$ for MgO) respectively (Makishima, 1973). The component oxides in this work are $R_2O_3$, $TiO_2$, $ZrO_2$, $Y_2O_3$, and $Al_2O_3$, and their dissociation energy is 60–70 kJ/cm$^3$, 86.5 kJ/cm$^3$, 97.0 kJ/cm$^3$, 74.0 kJ/cm$^3$, and 133.8 kJ/cm$^3$, respectively (Makishima, 1973; Inaba et al., 2000), which is much larger than that of conventional oxide glasses. Additionally, in the prepared high-entropy glasses, the content of

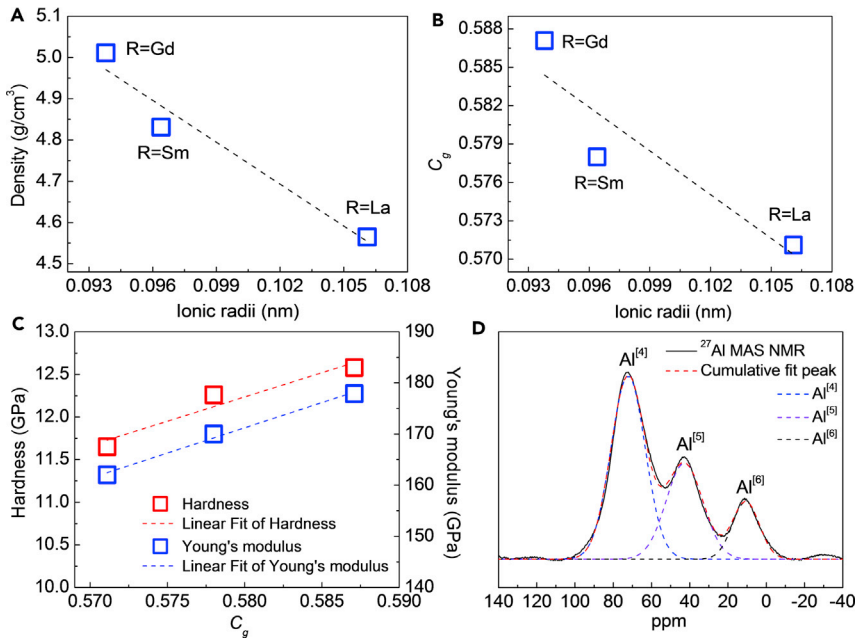


**Figure 6. Structure analysis of hardness and Young's modulus of the high-entropy $18.77R_2O_3$-$4.83Y_2O_3$-$28.22TiO_2$-$8.75ZrO_2$-$39.43Al_2O_3$ (R = La, Sm, Gd) glasses**

(A) Effect of the ionic radii of R (R = La, Sm, Gd) cations on the density ($\rho$) of glass samples.

(B) Effect of the ionic radii of R (R = La, Sm, Gd) cations on the atomic packing density ($C_g$) of glass samples.

(C) Effect of the atomic packing density ($C_g$) on Young's modulus and Vickers hardness of glass samples.

(D) 27Al NMR spectroscopy of the high-entropy R = La glass. The black line and red dash line are the experimental curve and the total fitting curve, respectively, and other three fitting dashes are blue dash ($Al^{[4]}$), green dash ($Al^{[5]}$), and black dash ($Al^{[6]}$). Results demonstrate that the high hardness and Young's modulus can be owing to the large cationic field strength of $Ti^{4+}$ and $Zr^{4+}$, the large dissociation energy of $Al_2O_3$, $TiO_2$, and $ZrO_2$, and the complex interaction between atoms due to the diversity of components.

$TiO_2$, $ZrO_2$, and $Al_2O_3$ (with high dissociation energy) is larger more than 80%, while the $B_2O_3$, $SiO_2$, and $P_2O_5$ (with lower dissociation energy than $TiO_2$, $ZrO_2$, and $Al_2O_3$) take the vast majority in the conventional oxide glasses, and the lower dissociation energy of the component oxides lead to the decreased fracture toughness of glass.

The coordination numbers of the commercial $B_2O_3$-, $SiO_2$-, and $P_2O_5$-based oxide glasses are usually 2–3, 1–4, and 1–3, respectively, and the higher coordination numbers are conducive to obtained tougher glass. As exhibited in Figure 6D, the fractions of $Al^{[4]}$, $Al^{[5]}$, and $Al^{[6]}$ are estimated to be 55.3%, 31.0%, and 13.7%, respectively, which are much higher than the values of commercial oxide glasses. Figure 7A shows the effect of entropy on the fracture toughness ($K_{IC}$) of oxide glasses (To et al., 2021; Yao, 2016; Scannell et al., 2017; Vullo and Davis, 2004; Wiederhorn et al., 1974; Mezeix, 2017; Kato et al., 2010; Reddy et al., 1988). Interestingly, although there are differences in composition, the fracture toughness values of glasses show a tendency of increases with the increase of entropy, which indicates that the fracture toughness of oxide glass may be related to entropy. The increased fracture toughness in a constant entropy on the areas where the upward arrows are located is due to the increased pressure during the preparation process, which translate the low coordinated B ($B^{[3]}$) and Al ($Al^{[4]}$) to high coordinated B ($B^{[4]}$) and Al ($Al^{[5]}$, $Al^{[6]}$), respectively (To et al., 2021). The improved fracture toughness by entropy may be speculated to the bending growth of cracks due to the complex interaction between atoms. For low-entropy glasses, it is usually composed of one or two major oxides and a small amount of other oxides; therefore, the types of coordinated atoms are monotonous. Once a crack is formed, it tends to extend in a line-like way owing to the structural similarity, as shown in Figure 7B. For high-entropy glasses, it is generally composed of five or more oxides, and the content of each oxide is thought to be between 5% and 35%, which increases the diversity of coordinated atoms and exhibits complex interaction between atoms. The structural multiplicity of high-entropy glass may increase the resistance of line-like crack extending and lead to bending growth, as

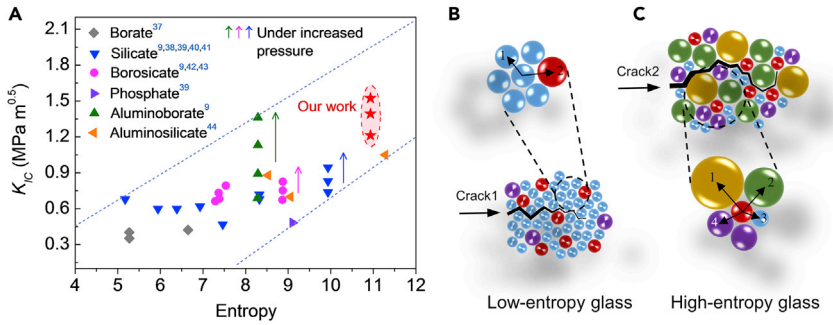


**Figure 7. Effect of entropy on the fracture toughness ($K_{IC}$) of oxide glasses**

(A) The fracture toughness of varying glasses, as obtained by means of various experimental methods as a function of entropy.

(B and C) Diagram of different styles of indentation crack extends and coordination situation in different entropy, and the crack 1 and crack 2 are corresponded to low entropy and high entropy, respectively.

Results demonstrate that the high fracture toughness can be owing to the large dissociation energy of $Re_2O_3$, $Al_2O_3$, $TiO_2$, and $ZrO_2$, the high coordinated Al, and the possible existence of bending growth of cracks caused by high entropy.

shown in Figure 7C. Under the constant external force, the bending growth of cracks may slow down the linear release of stress and thus results in an increase in fracture toughness.

## Conclusion

The mechanical and optical properties of high-entropy $18.77R_2O_3$-$4.83Y_2O_3$-$28.22TiO_2$-$8.75ZrO_2$-$39.43Al_2O_3$ (R = La, Sm, Gd) glasses prepared by an aerodynamic levitation technique are investigated. The glass of R = La and Gd is colorless and transparent in the visible region, meanwhile, displaying excellent optical properties. The density of glasses increases with the decrease of the ionic radii, and the atomic packing density $C_g$ increases with the decrease of the ionic radii. Results demonstrate that the ionic radii size has a great influence on the atomic packing density $C_g$. The Young's modulus and Vickers hardness are monotonically increased with the packing density $C_g$, and the measured $E$ and $H_V$ values of R = Gd glass are 177.9 GPa and 12.58 GPa, respectively, which exhibits the highest hardness and Young's modulus among oxide glasses. The prepared samples possess extraordinary fracture toughness among oxide glasses (1.21–1.52 MPa·m$^{0.5}$). The high atomic packing density $C_g$ is attributed to the addition of $Ti^{4+}$ and $Zr^{4+}$ cations, which possess high field strength. Accordingly, the high atomic packing density $C_g$, the large dissociation energy of $Al_2O_3$, $TiO_2$, and $ZrO_2$, and the complex interaction between atoms due to the diversity of the components are all contributing to the improvement of hardness and Young's modulus of glass. The high fracture toughness can be owing to the large dissociation energy of $Re_2O_3$, $Al_2O_3$, $TiO_2$, and $ZrO_2$, the high coordinated Al, and the possible existence of bending growth of cracks caused by high entropy.

The obtained results allow us to give some suggestions on enabling oxide glasses that have intrinsically high hardness, high Young's modulus, and high fracture toughness: (i) employing oxides with large dissociation energy, such as $Al_2O_3$, $ZrO_2$, and $TiO_2$, (ii) employing oxides with high field strength, such as $ZrO_2$ and $TiO_2$, e.g., to improve the coordination numbers, and (iii) increase the entropy of the system by adjusting the amount of different oxides when (i) and (ii) are determined. We believe that the successfully synthesized high-entropy glass in this work can offer a great opportunity to design new high hardness, high Young's modulus, and high fracture toughness oxide glasses.

## LIMITATIONS OF THE STUDY

In this work, the conceptual design of high-entropy materials is generalized to oxide glasses and successfully prepared the ultrahigh hardness, Young's modulus, and fracture toughness oxide glass with the compositions of $18.77R_2O_3$-$4.83Y_2O_3$-$28.22TiO_2$-$8.75ZrO_2$-$39.43Al_2O_3$ (R = La, Sm, Gd). However, the size of glass samples is still relatively small due to the limitation of the containerless melting approach. Considering the applications, the next step will be to explore the large size preparation of the glass. We have previously expanded the samples obtained by the containerless melting approach to the centimeter scale by hot pressing (Wang et al., 2019; Han et al., 2019), which can meet the requirements of

cover glass for some small wearable devices, such as smart watches. Additionally, we can also improve the glass-forming ability and reduce the melting point of glass by adding some of other oxides, such as silicon oxide and alkali metal oxide, so that the new glass can be prepared by the conventional melt-quenching methods.

## STAR★METHODS

Detailed methods are provided in the online version of this paper and include the following:

- KEY RESOURCES TABLE
- RESOURCE AVAILABILITY
  - Lead contact
  - Materials availability
  - Data and code availability
- METHOD DETAILS
  - Materials and glass synthesis
  - Characterization and testing
  - Calculation of the entropy S
  - Calculation of the fracture toughness $K_{IC}$
  - Calculation of the atomic packing density $C_g$

## ACKNOWLEDGMENTS

This work was financially supported by the Beijing Municipal Science and Technology Project (No. Z191100004819002), National Natural Science Foundation of China (No. 51972304), and the Project of Scientific Experiment on Chinese Manned Space Station. J.L. also specially acknowledged Professor D. Jiang and Professor J. Yu (Shanghai Institute of Ceramics, Chinese Academy of Sciences), Professor Y. Wu (University of Science and Technology Beijing), and Professor J. Gong (Tsinghua University) for their helpful discussion and suggestions.

## AUTHOR CONTRIBUTIONS

Conceptualization, J.L. and Y.G.; methodology, J.L. and Y.G.; formal analysis, Y.G.; investigation, Y.G., Y.Z., and S.F.; resources, S.F. and H.S.; writing-original draft, Y.G.; writing-review & editing, J.L., Y.G., and Y.Z.; supervision, J.L. and Y.G.; project administration, Y.G.; funding acquisition, J.L.

## DECLARATION OF INTERESTS

The authors declare no competing interests.

Received: May 17, 2021
Revised: June 6, 2021
Accepted: June 8, 2021
Published: July 23, 2021

## REFERENCES

Anstis, G.R., Chantikul, P., Lawn, B.R., and Marshall, D.B. (1981). A critical evaluation of indentation techniques for measuring fracture toughness: I, direct crack measurements. J. Am. Ceram. Soc. *64*, 533–538. https://doi.org/10.1111/j.1151-2916.1981.tb10320.x.

Argon, A.S. (1979). Plastic deformation in metallic glasses. Acta Mater. *27*, 47–50. https://doi.org/10.1016/0001-6160(79)90055-5.

Chen, C., Pang, S., Yang, Y., and Cheng, T.Z. (2015). A centimeter-size $Zr_{40}Hf_{10}Ti_4Y_1Al_{10}Cu_{25}Ni_7Co_2Fe_1$ bulk metallic glass with high mixing entropy designed by multi-substitution. J. Non Cryst. Sol. *410*, 39–42. https://doi.org/10.1016/j.jnoncrysol.2014.11.032.

Cheng, K.H., Lai, C.H., Lin, S.J., and Yeh, J.W. (2006). Recent progress in multi-element alloy and nitride coatings sputtered from high-entropy alloy targets. Ann. Chim. Sci. Mat. *31*, 723–736. https://doi.org/10.3166/acsm.31.723-736.

Dériano, S., Jarry, A., Rouxel, T., Sangleboeuf, J.C., and Hampshire, S. (2004). The indentation fracture toughness (KC) and its parameters: the case of silica-rich glasses. J. Non Cryst. Sol. *344*, 44–50. https://doi.org/10.1016/j.jnoncrysol.2004.07.021.

Du, J. (2009). Molecular dynamics simulations of the structure and properties of low silica yttrium aluminosilicate glasses. J. Am. Ceram. Soc. *92*, 87–95. https://doi.org/10.1111/j.1551-2916.2008.02853.x.

Del Grosso, M.F., Bozzolo, G., and Mosca, H.O. (2012). Determination of the transition to the high-entropy regime for alloys of refractory elements. J. Alloys Compd. *534*, 25–31. https://doi.org/10.1016/j.jallcom.2012.04.053.

Han, J., Wang, Z., Li, J., Li, X., and Xie, J. (2019). Large-sized $La_2O_3$-$TiO_2$ high refractive glasses with low $SiO_2$ fraction by hot-press sintering. Int. J. Appl. Glass. Sci. *10*, 371–377. https://doi.org/10.1111/ijag.13154.

Hehlen, M.P., Cockroft, N.J., Gosnell, T.R., Bruce, A.J., and Shmulovich, J. (1997). Uniform upconversion in high-concentration $Er^{3+}$-doped soda lime silicate and aluminosilicate glasses. Opt. Lett. *22*, 722–774. https://doi.org/10.1364/OL.22.000772.

Inaba, S., Todaka, S., Ohta, Y., and Morinaga, K. (2000). Equation for estimating the Young's modulus, shear modulus and Vickers hardness of aluminosilicate glasses. J. Jpn. Inst. Met. *64*, 177–183. https://doi.org/10.2320/jinstmet1952.64.3_177.

Johnson, J., Weber, R., and Grimsditch, M. (2005). Thermal and mechanical properties of rare-earth aluminate and low-silica aluminosilicate optical glasses. J. Non Cryst. Sol. *351*, 650–655. https://doi.org/10.1016/j.jnoncrysol.2005.01.065.

Kato, Y., Yamazaki, H., Yoshida, S., and Matsuoka, J. (2010). Effect of densification on crack initiation under Vickers indentation test. J. Non Cryst. Sol. *356*, 1768–1773. https://doi.org/10.1016/j.jnoncrysol.2010.07.015.

Kim, J.T., Hong, S.H., Park, J.M., Eckert, J., and Kim, K.B. (2020). New para-magnetic $(CoFeNi)_{50}(CrMo)_{50-x}(CB)_x$ (x = 20, 25, 30) non-equiatomic high-entropy metallic glasses with wide supercooled liquid region and excellent mechanical properties. J. Mater. Sci. Technol. *43*, 135–143. https://doi.org/10.1016/j.jmst.2020.01.004.

Li, A., and Zhang, X. (2009). Thermodynamic analysis of the simple microstructure of AlCrFeNiCu high-entropy alloy with multi-principal elements. Acta Metall. Sin. *22*, 219–224. https://doi.org/10.1016/S1006-7191(08)60092-7.

Li, R.X., and Zhang, Y. (2017). Entropy and glass formation. Acta Phys. Sin. *66*, 177101. https://doi.org/10.7498/aps.66.177101.

Li, X., Li, J., Li, J., Lin, H., and Li, B. (2017). Upconversion $32Nb_2O_5$-$10La_2O_3$-$16ZrO_2$ glass activated with $Er^{3+}/Yb^{3+}$ and dye sensitized solar cell application. J. Adv. Ceram. *6*, 312–319. https://doi.org/10.1007/s40145-017-0243-3.

Licheron, M., Montouillout, V., Millot, F., and Neuville, D.R. (2011). Raman and 27Al NMR structure investigations of aluminate glasses: (1-x) $Al_2O_3$-xMO, with M=Ca, Sr, Ba and 0.5<x<0.75. J. Non Cryst. Sol. *357*, 2796–2801. https://doi.org/10.1016/j.jnoncrysol.2011.03.001.

Lucas, M.S., Wilks, G.B., Mauger, L., Munoz, J.A., Senkov, O.N., Michel, E., Horwath, J., Semiatin, S.L., Stone, M.B., Abernathy, D.L., et al. (2012). Absence of long-range chemical ordering in equimolar FeCoCrNi. Appl. Phys. Lett. *100*, 251907. https://doi.org/10.1063/1.4730327.

Ma, X., Peng, Z., and Li, J. (2015). Effect of $Ta_2O_5$ substituting on thermal and optical properties of high refractive index $La_2O_3$-$Nb_2O_5$ glass system prepared by aerodynamic levitation method. J. Am. Ceram. Soc. *98*, 770–773. https://doi.org/10.1111/jace.13384.

Makishima, A. (1973). Mackenzie. Direct calculation of Young's modulus of glass. J. Non Cryst. Sol. *12*, 35–45. https://doi.org/10.1016/0022-3093(73)90053-7.

Mezeix, P. (2017). Verres et vitrocéramiques du système BaO-TiO2-SiO2: Propriétés mécaniques et couplage électromécanique (Universite de Rennes 1), PhD thesis.

Morozumi, H., Nakano, H., Yoshida, S., and Matsuoka, J. (2015). Crack initiation tendency of chemically strengthened glasses. Int. J. Appl. Glass. Sci. *6*, 64–71. https://doi.org/10.1111/ijag.12089.

Neuville, D.R., Cormier, L., and Massiot, D. (2006). Al coordination and speciation in calcium aluminosilicate glasses: effects of composition determined by 27Al MQ-MAS NMR and Raman spectroscopy. Chem. Geol. *229*, 173–185. https://doi.org/10.1016/j.chemgeo.2006.01.019.

Ng, C., Guo, S., Luan, J., Shi, S., and Liu, C.T. (2012). Entropy-driven phase stability and slow diffusion kinetics in an $Al_{0.5}$CoCrCuFeNi high-entropy alloy. Intermetallics *31*, 165–172. https://doi.org/10.1016/j.intermet.2012.07.001.

Nordberg, M.E., Mochel, E.L., Garfinkel, H.M., and Olcott, J.S. (1964). Strengthening by ion exchange. J. Am. Ceram. Soc. *47*, 215–219. https://doi.org/10.1111/j.1151-2916.1964.tb14399.x.

Østergaard, M.B., Hansen, S.R., Januchta, K., To, T., Rzoska, S.J., Bockowski, M., Bauchy, M., and Smedskjaer, M.M. (2019). Revisiting the dependence of Poisson's ratio on liquid fragility and atomic packing density in oxide glasses. Materials *12*, 2439. https://doi.org/10.3390/ma12152439.

Pahari, B., Iftekhar, S., Jaworski, A., Okhotnikov, K., Jansson, K., Stevensson, B., Grins, J., and Edén, M. (2012). Composition-property-structure correlations of scandium aluminosilicate glasses revealed by multinuclear 45Sc, 27Al, and 29Si solid-state NMR. J. Am. Ceram. Soc. *95*, 2545–2553. https://doi.org/10.1111/j.1551-2916.2012.05288.x.

Quinna, G.D., and Swab, J.J. (2013). Fracture toughness of glasses as measured by the SCF and SEPB methods. J. Eur. Ceram. Soc. *37*, 4243–4257. https://doi.org/10.1016/j.jeurceramsoc.2017.05.012.

Ranganathan, S. (2003). Alloyed pleasures: multimetallic cocktails. Curr. Sci. *85*, 1404–1406.

Reddy, K.P.R., Fontana, E.H., and Helfinstine, J. (1988). Fracture toughness measurements of glass and ceramic materials using chevron-notched specimens. J. Am. Ceram. Soc. *71*, C310–C313. https://doi.org/10.1111/j.1151-2916.1988.tb05911.x.

Rosales-Sosa, G.A., Masuno, A., Higo, Y., Inoue, H., Yanaba, Y., Mizoguchi, T., Umada, T., Okamura, K., Kato, K., and Watanabe, Y. (2015). High Elastic Moduli of a $54Al_2O_3$-$46Ta_2O_5$ glass fabricated via containerless processing. Sci. Rep. *5*, 15233. https://doi.org/10.1038/srep15233.

Rosales-Sosa, G.A., Masuno, A., Higo, Y., and Inoue, H. (2016). Crack-resistant Al2O3-SiO2 glasses. Sci. Rep. *6*, 23620. https://doi.org/10.1038/srep23620.

Rosales-Sosa, G.A., Masuno, A., Higo, Y., Watanabe, Y., and Inoue, H. (2018). Effect of rare-earth ion size on elasticity and crack initiation in rare-earth aluminate glasses. J. Am. Ceram. Soc. *101*, 5030–5036. https://doi.org/10.1111/jace.15760.

Rouxel, T., and Yoshida, S. (2017). The fracture toughness of inorganic glasses. J. Am. Ceram. Soc. *100*, 4374–4396. https://doi.org/10.1111/jace.15108.

Scannell, G.W., Laille, D.C., Celarie, F., Huang, L., and Rouxel, T. (2017). Interaction between deformation and crack initiation under Vickers indentation in $Na_2O$-$TiO_2$-$SiO_2$ glasses. Front. Mater. *4*, 6. https://doi.org/10.3389/fmats.2017.00006.

Schmücker, M., Schneider, H., Mackenzie, K.J.D., and Okuno, M. (1999). Comparative 27Al NMR and LAXS studies on rapidly quenched aluminosilicate glasses. J. Eur. Ceram. Soc. *19*, 99–103. https://doi.org/10.1016/S0955-2219(98)00181-2.

Segawa, H., Igarashi, T., Sakamoto, T., Mizuno, K., Konishi, T., and Inoue, S. (2010). Exploration of high-hardness/low-melting borate glasses. Int. J. Appl. Glass. Sci. *1*, 378–387. https://doi.org/10.1111/j.2041-1294.2010.00034.x.

Senkov, O.N., Wilks, G.B., Miracle, D.B., Chuang, C.P., and Liaw, P.K. (2010). Refractory high-entropy alloys. Intermetallics *18*, 1758–1765. https://doi.org/10.1016/j.intermet.2010.05.014.

Shannon, R.D., and Prewitt, C.T. (1969). Effective ionic radii in oxides and fluorides. Acta Cryst. *B25*, 925–946. https://doi.org/10.1107/S0567740869003220.

Stevensson, B., and Edén, M. (2013). Structural rationalization of the microhardness trends of rare-earth aluminosilicate glasses: interplay between the RE3+ field-strength and the aluminum coordinations. J. Non Cryst. Sol. *378*, 163–167. https://doi.org/10.1016/j.jnoncrysol.2013.06.013.

Sun, K.H. (1947). Fundamental condition of glass formation. J. Am. Ceram. Soc. *30*, 277–281. https://doi.org/10.1111/j.1151-2916.1947.tb19654.x.

Takahashi, S., Neuville, D.R., and Takebe, H. (2015). Thermal properties, density and structure of percalcic and peraluminus $CaO$-$Al_2O_3$-$SiO_2$ glasses. J. Non Cryst. Sol. *411*, 5–12. https://doi.org/10.1016/j.jnoncrysol.2014.12.019.

Tangeman, J.A., Phillips, B.L., Nordine, P.C., and Weber, J.K.R. (2004). Thermodynamics and structure of single- and two-phase yttria-alumina glasses. J. Phys. Chem. B *108*, 10663–10671. https://doi.org/10.1021/jp027779e.

To, T. (2019). Fracture toughness and fracture energy of inorganic and non-metallic glass (Universite de Rennes 1), PhD thesis.

To, T., Sorensen, S.S., Christensen, J.F.S., Christensen, R., Jensen, L.R., Bockowski, M., Bauchy, M., and Smedskjaer, M.M. (2021). Bond switching in densified oxide glass enables record-high fracture toughness. ACS Appl. Mater. Inter. *13*, 17753–17765. https://doi.org/10.1021/acsami.1c00435.

Tong, C.J., Chen, Y.L., Yeh, J.W., Lin, S.J., Chen, S.K., Shun, T.T., Tsau, C.H., and Chang, S.Y. (2005). Microstructure characterization of $Al_x$CoCrCuFeNi high-entropy alloy system with multiprincipal elements. Metall. Mater. Trans. A *36*, 881–893. https://doi.org/10.1007/s11661-005-0283-0.

Tsai, K.Y., Tsai, M.H., and Yeh, J.W. (2013). Sluggish diffusion in Co–Cr–Fe–Mn–Ni

high-entropy alloys. Acta Mater. *61*, 4887–4897. https://doi.org/10.1016/j.actamat.2013.04.058.

Vullo, P., and Davis, M.J. (2004). Comparative study of micro-indentation and Chevron notch fracture toughness measurements of silicate and phosphate glasses. J. Non Cryst. Sol. *349*, 180–184. https://doi.org/10.1016/j.jnoncrysol.2004.08.181.

Wang, Z., Han, J.J., Li, J.Q., Li, X.Y., Li, J.T., He, G., and Xie, J. (2019). Plastic sintering behavior of large-sized $La_2O_3$-$TiO_2$-$ZrO_2$ amorphous bulk. J. Inorg. Mater. *34*, 433–438. https://doi.org/10.15541/jim20180289.

Wiederhorn, S.M., Johnson, H., Diness, A.M., and Heuer, A.H. (1974). Fracture of glass in vacuum. J. Am. Ceram. Soc. *57*, 336–341.

Yamane, M., and Mackenzie, J.D. (1974). Vicker's hardness of glass. J. Non Cryst. Sol. *15*, 153–164. https://doi.org/10.1016/0022-3093(74)90044-1.

Yao, Z.Y. (2016). Synthesis, structure, and mechanical properties of lead and zinc-copper borate glasses (Universite de Rennes 1), PhD thesis.

Yeh, J.W. (2006). Recent progress in high-entropy alloys. Ann. Chim. Sci. Mat *31*, 633–648. https://doi.org/10.3166/acsm.31.633-648.

Yeh, J.W., Chen, S.K., Lin, S.J., Gan, J.Y., Chin, T.S., Shun, T.T., Tsau, C.H., and Chang, S.Y. (2004). Nanostructured high-entropy alloys with multiple principal elements: novel alloy design concepts and outcomes. Adv. Eng. Mater. *6*, 299–303. https://doi.org/10.1002/adem.200300578.

Zhao, Z.F., Xiang, H.M., Chen, H., Dai, F.Z., Wang, X.H., Peng, Z.J., and Zhou, Y.C. (2020). High-entropy $(Nd_{0.2}Sm_{0.2}Eu_{0.2}Y_{0.2}Yb_{0.2})_4Al_2O_9$ with good high temperature stability, low thermal conductivity, and anisotropic thermal expansivity. J. Adv. Ceram. *9*, 595–605. https://doi.org/10.1007/s40145-020-0399-0.

# STAR★METHODS

## KEY RESOURCES TABLE

| REAGENT or RESOURCE | SOURCE | IDENTIFIER |
|---|---|---|
| Chemicals, peptides, and recombinant proteins | | |
| $La_2O_3$ | Sinopharm chemical reagent co. ltd | Cat# 52003861 |
| $Gd_2O_3$ | Sinopharm chemical reagent co. ltd | Cat# 52002964 |
| $TiO_2$ | Sinopharm chemical reagent co. ltd | Cat# 51026992 |
| $Y_2O_3$ | Sinopharm chemical reagent co. ltd | Cat# 52007264 |
| $Sm_2O_3$ | Aladdin chemical reagent co. ltd | Cat# S108775 |
| $ZrO_2$ | Aladdin chemical reagent co. ltd | Cat# 2104398 |
| $Al_2O_3$ | Aladdin chemical reagent co. ltd | Cat# A140802 |
| Other | | |
| X-ray diffractometer | Rigaku Corporation | Smartlab 9 |
| Differential thermal analyzer | NETZSCH | STA499F3 |
| Field Emission scanning electron Microscope | JEOL | JSM-7610F |
| UV-VIS-NIR spectrophotometer | Varian | Cary 5000 |
| Fourier transform infrared spectrometer | Varian | FTIR Excalibur 3100 |
| Nanoindenter | Keysight technologie | G200 |
| Vickers hardness tester | Shanghai Jvjing Precision Instrument Manufacturing Co., Ltd | HV-1000IS |
| JNM-ECZ600R spectrometer | JEOL | JNM-ECA600 |

## RESOURCE AVAILABILITY

### Lead contact

Further information and requests for resources and reagents should be directed to and will be fulfilled by the lead contact, Jianqiang Li (jqli@ipe.ac.cn).

### Materials availability

This study did not generate new unique reagents.

### Data and code availability

- All data reported in this paper will be shared by the lead contact upon request.
- This paper does not report original code.
- Any additional information required to reanalyze the data reported in this paper is available from the lead contact upon request.

## METHOD DETAILS

### Materials and glass synthesis

Glasses were fabricated by an aerodynamic levitator equipped with laser heating (Li et al., 2017). The details of the preparation of glass by aerodynamic levitator is shown below. High purity oxide powders $La_2O_3$, $Gd_2O_3$, $TiO_2$, $Y_2O_3$ (Sinopharm chemical reagent co. ltd, 99.99% purity) and $Sm_2O_3$, $ZrO_2$, $Al_2O_3$ (Aladdin chemical reagent co. ltd, 99.99% purity) were used as raw materials and mixed stoichiometrically with the nominal composition of $18.77R_2O_3$-$4.83Y_2O_3$-$28.22TiO_2$-$8.75ZrO_2$-$39.43Al_2O_3$ (R = La, Sm, Gd) in molar ratio. Then, the well mixed powders were pressed into pellets and crumbled into small pieces. Prior to synthesis, all pieces were pre-sintered at 600°C for 2 hr in air to increase pieces' strength. Pieces of ~60–200 mg were then levitated on the nozzle of an ADL furnace by oxygen flow and heated to melt by three $CO_2$ lasers. Keeping the molten state for 10–20 s to ensure homogeneity, then turning off the laser to rapid solidification. The obtained samples (beads with 3 mm in diameter) were colorless and transparent.

### Characterization and testing

The structure of glass samples was identified by X-ray diffraction (XRD, Smartlab 9, Rigaku Corporation, Tokyo, Japan). The glass transition temperature $T_g$ and onset crystallization temperature $T_p$ were measured by a differential scanning calorimeter (Differential thermal analysis (DTA), STA499F3, NETZSCH, Selb, Germany) from room temperature to 1200°C at a heating rate of 10°C/min in Ar atmosphere. Field Emission Scanning Electron Microscope (FE-SEM, JSM-7610F, Tokyo, Japan) with energy dispersive spectroscopy (EDS) were used to verify the homogeneity of the element distribution. Prior to SEM observation, the bead glass samples were polished to pellet on both sides and the cleaned pellets were then sputtered carbon coating for a better conductivity. The accelerating voltage and probe current of SEM were 15 kV and 8, respectively. The transmittance spectrum of glass in 190–2500 nm and 2500–8000 nm wavelength range were obtained by UV-VIS-NIR spectrophotometer (Cary 5000, Varian, America) and Fourier transform infrared spectrometer (FTIR Excalibur 3100, Varian, America), respectively. Before measurement, glass samples were double polished and cleaned up (1.0 mm in thickness). The density was measured using a gas pycnometer (Micromeritics Accupyc II 1340, Atlanta, GA). The hardness and Young's modulus of the samples was measured by nanoindenter (Keysight technologie-G200) with a depth of 2000 nm, each samples were carried out at least three indentations using a diamond indenter. The fracture toughness was measured by a Vickers hardness tester (Shanghai Jvjing Precision Instrument Manufacturing Co., Ltd, Shanghai, China) under a load of 49 N with a loading time of 10 s. In order to increase the accuracy of measurement, each samples were carried out at least nine indentations using a diamond indenter in different areas, all measurements were performed at 25°C with a relative humidity of 50%. To identify the coordination information of glass samples, $^{27}$Al NMR spectroscopy was performed on a JNM-ECZ600R spectrometer (JEOL, Tokyo, Japan). The spinning rate was 12 kHz and a 3.2 mm diameter zirconia tube was used. The relaxation delay and scanning time were 5 s and 1 hr, respectively. The $^{27}$Al chemical shift in ppm was referenced to an external 1 M $AlCl_3$ solution.

### Calculation of the entropy S

The entropy $S$ of the high-entropy glass samples are calculated by the formula:

$$S = -R\sum_{i=1}^{N} x_i \ln x_i$$

Where R is the molar gas constant, $x_i$ is the mole fraction of cation i, $N$ is the number of cations.

### Calculation of the fracture toughness $K_{IC}$

The fracture toughness $K_{IC}$ of the high-entropy glass samples are calculated by the formula (Anstis et al., 1981):

$$K_{IC} = 0.016\left(\frac{E}{H_V}\right)^{0.5}\frac{P}{c^{1.5}}$$

Where $E$ is the Young's modulus, $H_V$ is the Vickers hardness, $P$ is the supplied load, $c$ is the average distance from the middle of the indentation to the end of the cracks.

### Calculation of the atomic packing density $C_g$

The atomic packing density $C_g$ of the high-entropy glass samples are calculated by the formula:

$$C_g = \frac{\rho\sum x_i V_i}{M}$$

Where $\rho$ is the measured density, $M$ is the molecular mass of the glass, $x_i$ is the molar fraction of oxide $i$, $V_i$ is the ionic volume of oxide $i$. The ionic volume is given by the formula:

$$V_i = N_A\frac{4}{3}\pi\left(m{r_A}^3 + n{r_O}^3\right)$$

Where $N_A$ is Avogadro's number, $m$ and $n$ are the number of atoms in the $A_mO_n$ oxide, $r_A$ and $r_O$ are the ionic radius of cation and oxygen, respectively. Shannon and Prewitt ionic radii are used (Shannon and Prewitt, 1969). The radius of the oxide ion is 1.35 Å.